



Performance of a prototype stationary catadioptric concentrating photovoltaic module

JOHN LLOYD,^{1*} MICHAEL PAVILONIS,¹ CHRISTOPHER GLADDEN,¹
CHADWICK CASPER,¹ KEVIN SCHNEIDER,¹ WILLIAM MCMAHON,²
AND PETER KOZODOY¹

¹*Glint Photonics, 1520 Gilbreth Ave. Burlingame CA 94410, USA*

²*National Renewable Energy Laboratory, Golden CO 80401, USA*

*jlloyd@glintphotonics.com

Abstract: A stationary catadioptric concentrating photovoltaic module with aperture area over 100 cm², geometric concentration of 180x, and collection within 60° of polar incidence was designed, prototyped, and characterized. The module performance followed modeling closely with a peak power conversion efficiency of 26% for direct irradiance. Tracking of the sun is accomplished via translational micro-tracking completely internal to the module, avoiding the cost and complexity of mechanical two-axis trackers that point towards the sun. This demonstrates the potential for concentrating photovoltaic modules with significantly higher efficiency than industry standard silicon photovoltaic modules that could be installed in stationary configurations on rooftops.

© 2018 Optical Society of America under the terms of the [OSA Open Access Publishing Agreement](#)

OCIS codes: (040.5350) Photovoltaic; (080.2740) Geometric optical design; (220.1770) Concentrators; (350.3950) Micro-optics; (350.6050) Solar energy.

References and links

1. A. Polman and H. A. Atwater, "Photonic design principles for ultrahigh-efficiency photovoltaics," *Nat. Mat.* **11**, 174-177 (2012).
2. M. A. Green, Y. Hishikawa, W. Warta, E. Dunlop, D. Levi, J. Hohl-Ebinger, and A. Ho-Baille, "Solar cell efficiency tables (version 50)," *Prog. in Photovoltaics*, **57**(7), 668-676 (2017).
3. K. Shanks, S. Senthilarasu, and T. K. Mallick, "Optics for concentrating photovoltaics: Trends, limits, and opportunities for materials and design," *Renewable and Sustainable Energy Reviews*, **60**, 349-407 (2016).
4. J. Hallas, K. A. Baker, J. H Karp, E. J. Tremblay, and J. E. Ford, "Two-axis solar tracking accomplished through small lateral translations," *Appl. Opt.* **51** 6117-6124 (2012).
5. P. Kozodoy, C. Gladden, M. Pavilonis, C. Rhodes, T. Wheeler, and C. Casper, "Self-Tracking Concentrator for Photovoltaics," in *CLEO: 2015, OSA Technical Digest* (online) (Optical Society of America, 2015), paper ATu2J.1.
6. J. Price, X. Sheng, B. Meulblok, J. A. Rogers, and N. C. Giebink, "Wide-angle planar microtracking for quasi-static microcell concentrating photovoltaics," *Nat. Comm.*, **6** 6223 (2015).
7. G. N. Nielson, M. Okandan, J. L. Cruz-Campa, A. L. Lentine, W. Sweatt, V. P. Gupta, and J. S. Nelson, "Leveraging scale effects to create next-generation photovoltaic systems through micro- and nanotechnologies," *Proc. SPIE* **8373**, 837317, (2012).
8. P. Espinet-González, I. Rey-Stolle, M. Ochoa, C. Algora, I. Garcia, and E. Barrigon, "Analysis of perimeter recombination in the subcells of GaInP/GaAs/Ge triple-junction solar cells," *Prog. in Photovoltaics*, **23**(7) 874-882 (2015).
9. J. S. Price, A. Grede, B. Wang, M. V. Lipski, K. Lee, J. He, G. S. Brulo, X. Ma, S. Burroughs, C. D. Rahn, R. G. Nuzzo, J. A. Rogers, and N. C. Giebink, "High-concentration planar microtracking photovoltaic system exceeding 30% efficiency," *Nat. Energy*, **2** 17113 (2017).

1. Introduction

Optical concentration of solar radiation offers the potential for photovoltaic module efficiencies well in excess of industry standard silicon photovoltaic modules by virtue of both the physics of the photovoltaic effect [1] and the opportunity to use higher efficiency photovoltaic materials [2] that are not economical or sustainable at one-sun concentration. Optical concentration is typically

achieved via geometric optics [3] that are mechanically oriented normal to direct solar radiation, but the nature of mechanical pointing makes it unattractive for deployment in areas where efficiency is most valued, namely rooftops and other area-constrained situations.

A stationary concentrating photovoltaic (CPV) module is possible, however, by entirely internal micro-scale translational focal spot tracking [4–6]. High concentration is achievable in a catadioptric design featuring an outward-facing refractive lens and an inward-facing reflective lens suitably designed such that the focal plane remains flat out to high angles of incidence. Tracking of the sun is accomplished by translating cells within the focal plane to receive the concentrated irradiance. The translational movements can be sufficiently short (mm-scale) such as to be completely internal to the module without adding appreciable area to the module. Module efficiencies approaching 40% for direct irradiance are conceivable, and even accounting for the fraction of available irradiance which is direct, this corresponds to a module with the same form factor and installation as standard silicon modules while capable of delivering up to 80% more energy on an annualized areal basis. In this work we report on progress toward the design and prototyping of a stationary catadioptric photovoltaic module with an aperture in excess of 100 cm².

2. System design

The stationary catadioptric concentrator involves an array of outward-facing refractive lenses in registry with an array of inward-facing reflective lenses, and is depicted in Fig. 1 (left). Light enters the refractive lenses and is concentrated onto the rear reflective lens, which concentrates it further onto an array of rearward facing cells mounted on a receiver tile between the two lens arrays. An inexpensive and chemically inert fluid is present between the two lens arrays to avoid undesirable Fresnel reflections at the various interfaces, as all materials within the optical path have a refractive index of approximately 1.5.

Figure 1 (right) depicts the wavelength dependent power loss of the optical system under normally-incident illumination of 1° half angle divergence by sequentially stacking loss mechanisms. The first source of loss is purely geometric, representing the shadowing of the cell as well as chromatic aberration at very short wavelengths. The next added loss comes from considering Fresnel reflections, dominated by the initial interface between air and uncoated acrylic. Next, the volumetric absorption of materials is considered as the optical path length within the system exceeds 1 cm. Fortunately, the significant absorptive losses at longer wavelengths are minor system efficiency losses, as several absorption bands overlay atmospheric absorption lines where there is little power in the incident spectrum. The non-unity reflectivity of the silver coating on the rear mirror is also included, and finally the shadowing of the electrical traces and heat spreading elements.

The geometric optics of the catadioptric concentrator are scale invariant, but there are physical and economic impacts that guide the system size [7]. A smaller optical system requires reduced volume of optical components, enables more efficient heat spreading from the cell, and requires a shorter throw for actuation. However, along with those benefits a smaller system size also dictates an increasing component count, reduced physical tolerances in the manufacturing and tracking, and eventually, significant sidewall recombination in the photovoltaic cells [8]. In accordance with these trade-offs, the optical system was designed with close-packed truncated hexagonal lenslets 2 cm in diameter allowing tracking to 60° polar incidence via 1.5 cm of translation. Photovoltaic cells available commercially and measuring 1.2 x 1.2 mm result in a geometric concentration of 180x.

The lens formulae were designed with Zemax ray-tracing software, and optimized for an alternative embodiment of the system where light is coupled into a waveguide rather than onto photovoltaic cells. The numerical aperture matching required by the former functionality restricted the performance as a photovoltaic concentrator, although the design is still capable

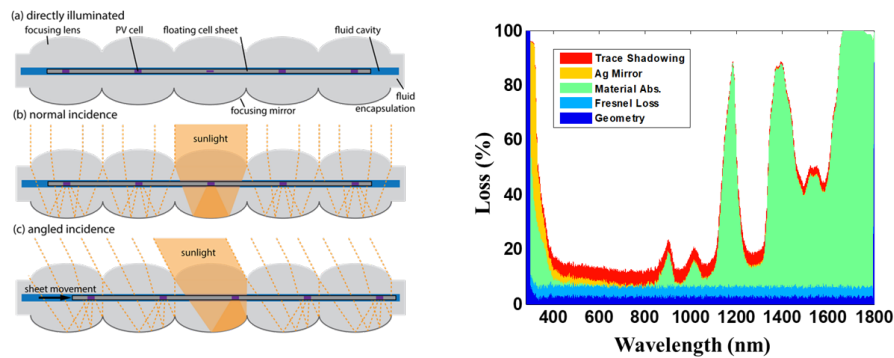


Fig. 1. **Left:** Operating principle of translational micro-tracking catadioptric concentrating photovoltaic module. a) Module components b) Collection of normally incident sunlight c) Collection of sunlight at non-normal incidence via translation of photovoltaic cells **Right:** Wavelength dependent losses from a series of accumulated mechanisms.

of good performance out to high angles of incidence. Ray-tracing simulations performed using Synopsys LightTools were used to predict optical performance and map the focal position of the system as a concentrating photovoltaic module.

The force required for lateral actuation of the receiver tile was designed to be transmitted magnetically by mounting the receiver tile within a carrier with four magnets embedded within it. This allows magnets to be attached on a flat area on the outer surface of the refractive lens array, outside the optical aperture of the system. Positioning these external magnets provides an attractive force to pull the carrier and receiver tile into registry. The external magnets can be positioned individually or embedded within a frame that maintains their relative positions and allows motion in unison.

Photovoltaic cells operate with reduced efficiency at increasing temperatures, and in this system the cells are exposed to concentrated irradiance while embedded within millimeters of fluid and polymer. The thermal resistance out of the module is thus higher than point-focus CPV modules with rear heat-sinks. In order to extract waste heat from the cell during operation it useful to reduce the in-plane thermal resistance, such that the vertical thermal resistance is parallelized and reduced. The receiver tile was designed for lateral heat spreading by the addition of metal traces emanating radially from the photovoltaic cell. These traces sit within the optical path, and thus their size must balance thermal losses and shadowing losses. These losses were balanced in this design by developing a finite element thermal model to determine the cell temperature for a given width and thickness of these heat spreading features. The thermal loss was then calculated from a lumped circuit element simulation performed in LTSpice of the photovoltaic cells at various temperatures. The width of the features was then set such that the thermal losses equaled the optical loss, with the chosen layout resulting in approximately 4.5% shadowed area.

Electrical current is also extracted along the metal traces, and along busbars that interconnect each unit cell. The front lens concentrates the incident light sufficiently that these interconnecting busbars are not illuminated and thus not a source of optical loss. This allows sufficiently wide busbars to interconnect the 42 cells in this design electrically in parallel with <1% electrical resistance losses in the traces. This parallel topology also protects mismatched photocurrents from cells from damaging reverse bias conditions. The optimal circuit topology including sufficient bypass diodes for larger modules is still a topic under development.

3. Prototype fabrication

A prototype module containing 42 hexagonally packed unit cells with 109 cm^2 of optical aperture was fabricated to validate the optical design and demonstrate performance of the photovoltaic cells under typical operating conditions. Elements of the prototype module are depicted in Fig. 2. The two lens arrays were compression molded with polymethyl methacrylate (PMMA), and the rear lens array was coated with a silver mirror. Alignment features in the mold ensured registry with high tolerance between the two lens arrays. The top and bottom lens arrays were joined by a compressive fixture and a gasket which retained the index matching fluid.

Triple-junction photovoltaic cells with 37.5% CSTC efficiency were attached to a transparent circuit produced via standard semiconductor processing techniques and electrically connected in parallel. Copper electrical traces were electroplated onto a 0.7 mm thick glass tile and capped with Ni/Au to facilitate wire bonding between the cell top contacts and the electrical traces. In addition to two electrode arms per cell to extract photocurrent, heat spreading arms were incorporated to laterally spread waste heat generated at the cell to maintain lower device operating temperatures. Conservative fabrication constraints limited the aspect ratio of these features to 0.5:1 (thickness:width), but increasing this ratio would improve the heat spreading without significant optical penalties.

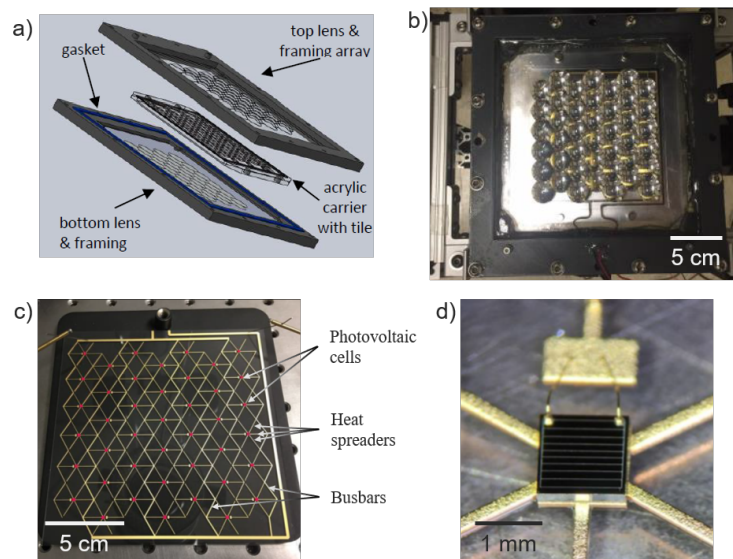


Fig. 2. Prototype module components: a) Exploded view of lens arrays with carrier tray and receiver tile b) Top view of assembled module with with clamping frame c) Receiver tile with 42 cells in position emitting light under forward bias d) Image of photovoltaic cell soldered onto electrical traces with wire bond connections

The glass tile containing the cells was held within a PMMA carrier tray, into which magnets were embedded to allow translation of the cells within the focal plane. The tray and tile were translated by attaching additional magnets to the exterior of the front lens array and translating those magnets. This actuation scheme had the advantage of simple manual motion control that avoided mechanical pass-throughs and associated sealing challenges. However, the stiction between the carrier tray and the optics proved to be quite limiting. Friction between sliding surfaces was minimized by application of fluorinated ethylene propylene (FEP) tape and embedding glass bearings into the carrier tray to minimize contact area. The motion was not continuous, and the combination of hysteresis and stick-slip motion was a major impediment to optimal

positioning of the cells within the focal plane that seems to be inherent to this method of magnetic translational positioning. Positioning was precise only to within approximately $500\ \mu\text{m}$, and thus measurements required repeated positioning attempt.

4. Module performance

The performance of the prototype module was evaluated using an Oriel 94123A-CPV Sol3A solar simulator with an AM1.5D spectral filter. The module was mounted on a plate attached to a two-axis telescope tracker head which was driven to an incident test angle. The position of the tray and tile within the module was adjusted by manual positioning of external magnets. The module was maintained at zero bias and the photocurrent was monitored in real-time while the sheet position was optimized. At the position of peak photocurrent a current-voltage trace was taken. Lamp output was normalized by measurements of the receiver tile removed from the module.

The measured photocurrent is recorded in Fig. 3, along with the modeled photocurrent resulting from the incident flux (both raw and incorporating the modeled optical efficiency of the system). The normal incidence measurement is the only data point that deviates appreciably from simulations, and this is explainable due to the difficulties associated with the magnetic actuation. The manual alignment procedure was most challenging at normal incidence because the operator could not assess the alignment visually without obscuring the incident beam. Thus, the measured system response at normal incidence is almost certainly unnecessarily low due to poor alignment of the receiver tile to the optics. This is directly a result of the stick-slip motion of the magnetic actuation, and is not fundamental to the optical system. Modules with direct mechanical drive of the receiver are under development that do not exhibit this limitation.

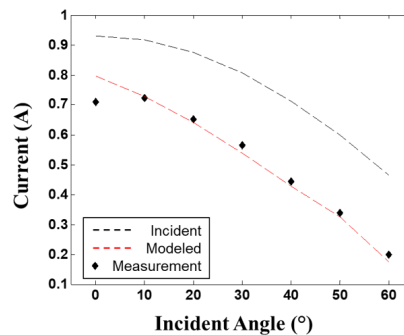


Fig. 3. Measured photocurrent of prototype module exposed to AM1.5D spectrum as a function of polar angle of incidence, along with the simulated (red dashed) and total incident (black dashed) photocurrent/flux.

The resulting I-V sweeps for angles of incidence out to 60° are shown in Fig. 4, along with the extracted module and cell power conversion efficiencies at the max power point of each curve. The normal incidence measurement yielded a slightly lower module efficiency, due in part to the optical alignment difficulty described above, but also in part to lower cell efficiency. The fill factor and voltage of the normal incidence measurement indicate a higher cell temperature than indicated at greater angles. This is consistent with the much longer measurement time where the cells were maintained at zero bias under illumination while the alignment was adjusted.

The average cell efficiency calculated from each measurement is reported in Fig. 4. This cell efficiency was calculated at each angle of incidence by dividing the measured module efficiency by the module optical efficiency as determined from the measured short circuit current. These cell

efficiencies are several absolute percentage points below their datasheet efficiency due primarily to their elevated temperature during test, as inferred from comparison of electrical measurements to a lumped circuit element electrical model of the module. Several factors caused cell temperatures during measurement to be approximately 90 °C. The module was held at zero bias and thus all incident power was dissipated as heat within the module for long periods during the alignment and test of the system. The module was also mounted flush against a polymer backing plate leaving no opportunity for natural convection on the rear of the module, an important heat extraction pathway. This highlights the importance of careful thermal design of the module to extract heat efficiently from cells embedded within a folded optical path. Limited testing of this module outdoors on a clear day under normally incident sunlight with 910 W/m² DNI and 22 °C air temperature resulted in cell temperatures of approximately 65 °C, a temperature consistent with thermal modeling, and cell efficiencies several percentage points higher than depicted in Fig. 4. It is noteworthy that despite the elevated operating temperature of the cells, differential thermal expansion between the glass receiver tile and the acrylic optics was negligible at this size scale. This is evidenced by the good agreement of measured short circuit current with modeling at most angles of incidence, which would not be the case if the registry of the arrays were not maintained.

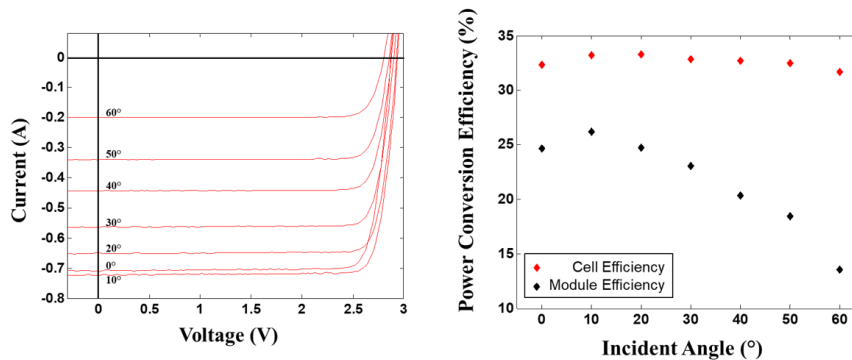


Fig. 4. **Left:** Current-Voltage behavior of prototype module for incident angles from 0° to 60°. Incident photocurrent falls approximately with the cosine of the angle. **Right:** Power conversion of efficiency of the module and photovoltaic cells with incident angle.

A fair performance comparison with one-sun silicon modules is challenging because of the nature of concentrating optics and geographic dependence of the direct normal incidence (DNI) resource. In silicon photovoltaics, module performance is rated at standard test conditions (STC) and the energy generated in an installation is quantified by a location-specific performance ratio that captures deratings from weather effects and system level losses. To simply yet fairly compare the technical merit of a stationary CPV module relative to a one-sun module without cumbersome system level modeling we report here an intermediate metric, intended to capture the angle-dependence of the CPV module without various system derates that are also not captured by the nominal STC efficiency of a silicon module. We therefore report the nominal stationary efficiency of our micro-tracking CPV module by integrating the angle-dependent DNI solar resource against the angle-dependent optical efficiency multiplied by the CSTC cell efficiency (37.5%). For the initial prototype presented here, that nominal stationary efficiency is 18% of total solar irradiance (DNI and diffuse) in high DNI locations such as Tucson, AZ and Reno, NV, and 13.5% in low-DNI Seattle. This number is significantly lower than its limiting potential due to lower optical efficiency at higher angles, and a moderately revised design that has been fabricated has a modeled nominal stationary efficiency of 22.5%. These both were not optimized for photovoltaic receivers, and we anticipate future prototypes with appropriately designed optics

and higher efficiency cells to yield nominal stationary efficiencies approaching 30% as has been demonstrated for single element systems [9].

5. Conclusion

The stationary concentrating photovoltaic module demonstrated in this work represents a promising step to developing a high efficiency concentrating photovoltaic module that overcomes critical limitations in previous commercialized concentrating photovoltaics. Namely, despite their high module efficiency, mechanical tracking by pointing modules towards the sun is ill-suited to area-constrained installations, which is where high efficiency is most valued. The design described here overcomes this critical limitation, and demonstrates that high-concentration can be achieved in stationary panels suitable for dense packing, while managing the thermal and electrical interconnection challenges associated with a photovoltaic cells embedded within a folded optical path. Initial, fairly crude, prototypes demonstrated efficiency greater than best-in-class silicon modules out to 30° of incidence, and appreciable efficiency out to 60° with a collection area greater than 100 cm². We expect that optimized optics and other planned design improvements will result in modules that significantly out-perform silicon photovoltaics on an energy-per-area basis. This technology has the potential to provide a valuable energy generating platform for rooftops and other applications.

Funding

Department of Energy (DOE) ARPA-E (DE-AR0000332, DE-AR0000644); California Energy Commission (CEC) (EPIC14-040).

Acknowledgments

We gratefully acknowledge funding for this work from ARPA-E through OPEN 2012 MOSAIC programs, as well as from the California Energy Commission through the EPIC program.